# Supporting Information

# Epidermis inspired ultrathin 3D cellular sensors array for self-powered biomedical monitoring

*Cheng Yan,[†] Weili Deng,[*,†] Long Jin,[†] Tao Yang,[†] Zixing Wang,[†] Xiang Chu,[†] Hai Su,[†]*

*Jun Chen,[*,‡] and Weiqing Yang[*,†,§]*

[†]Key Laboratory of Advanced Technologies of Materials (Ministry of Education), School of Materials Science and Engineering, Southwest Jiaotong University, Chengdu 610031, China

[§]State Key Laboratory of Traction Power, Southwest Jiaotong University, Chengdu 610031, China

[‡]Department of Materials Science and Engineering, Stanford University, Stanford, California 94305, USA.

**Corresponding Author**

*E-mail: weili1812@swjtu.edu.cn

*E-mail: chenjun@stanford.edu

*E-mail: wqyang@swjtu.edu.cn

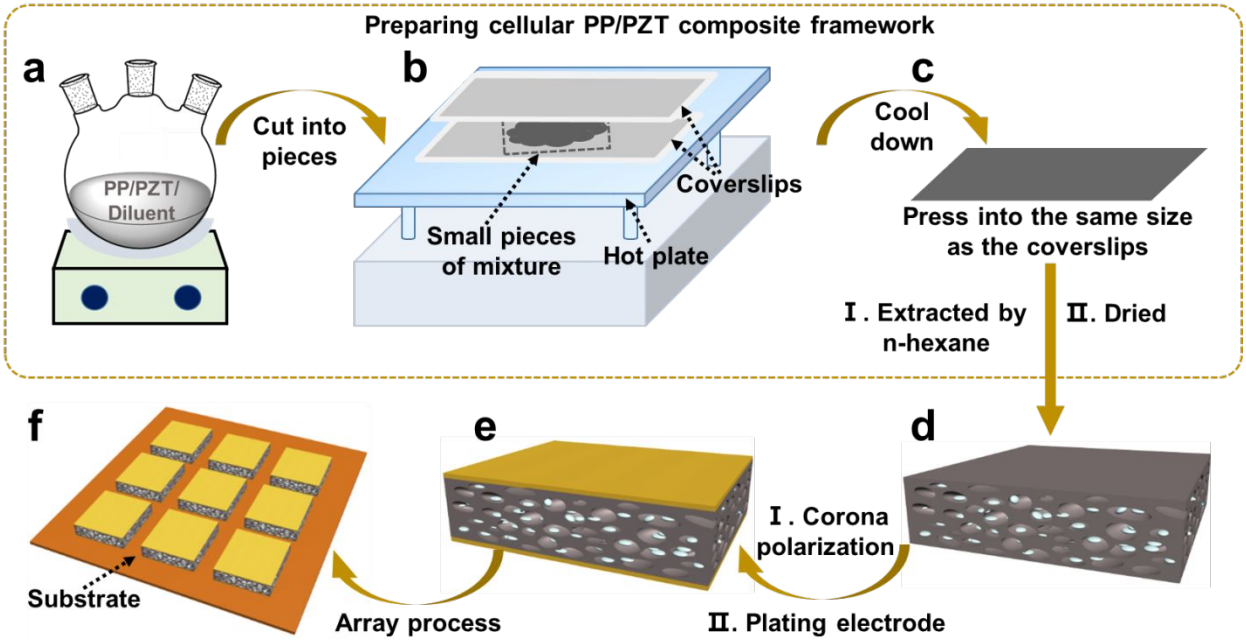


**Figure S1.** The schematic illustration showing the fabrication process of the three-dimensional cellular sensors array (3D-CSA). **(a)** Three components mixed in a three-necked flask for yielding a homogeneous solution. **(b)** The pieces of mixture placing on the coverslips and **(c)** spread into a film. **(d)** The cellular PP/PZT composite framework. **(e)** The fabricated sensor. **(f)** The 3 by 3 units of array on the kapton substrate.

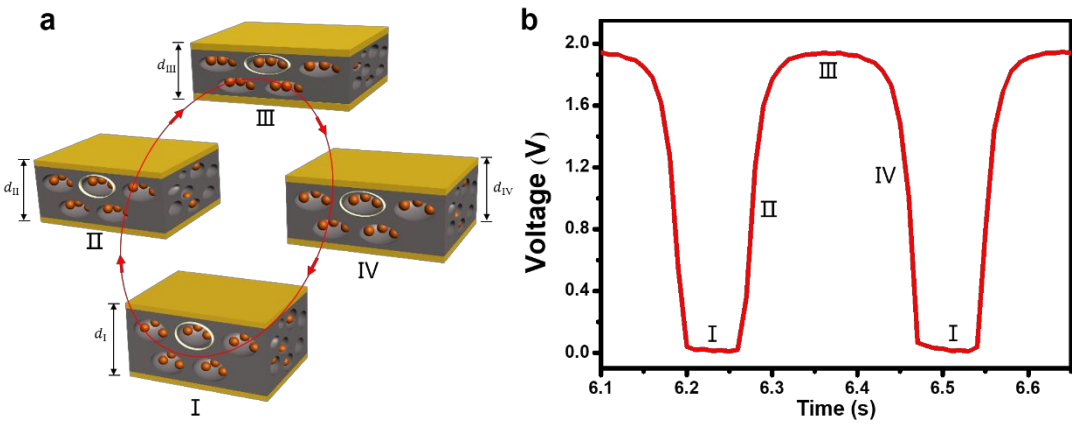


**Figure S2. (a)** Working mechanism of a 3D-CSA when it is at four stages: Ⅰ the original, Ⅱ the pressing, Ⅲ the equilibrium, Ⅳ the releasing. **(b)** Enlarged view of the open-circuit voltage of a 3D-CSA in one period corresponding to four stages.

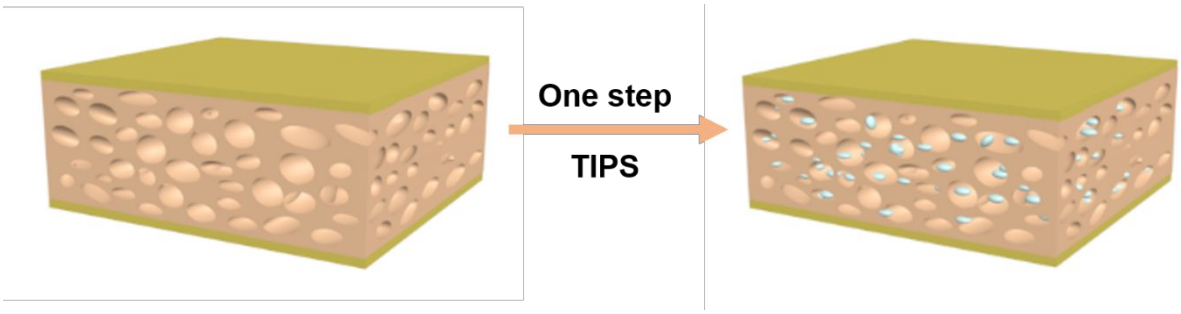


**Figure S3.** Sketch showing the one-step thermally induced phase separation method (TIPS), which is simple, straightforward and scalable.

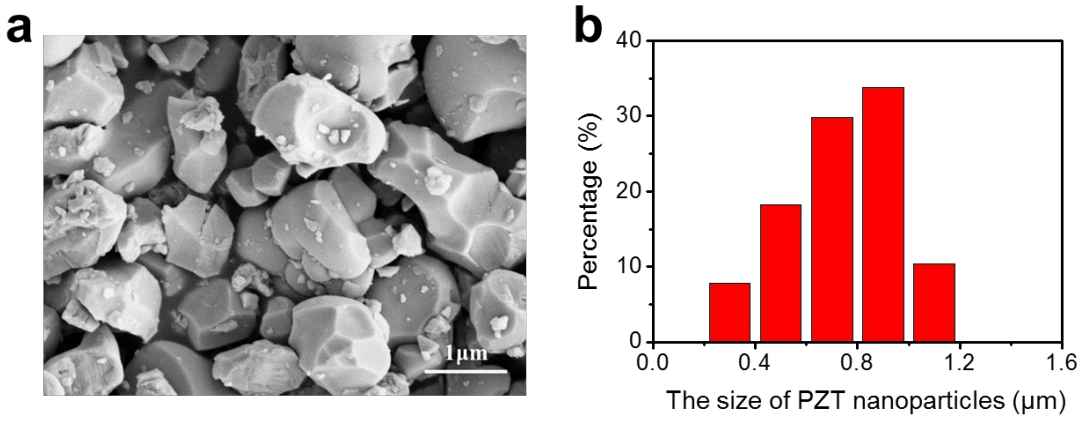


**Figure S4. (a)** SEM image and **(b)** size distribution of PZT nanoparticles.

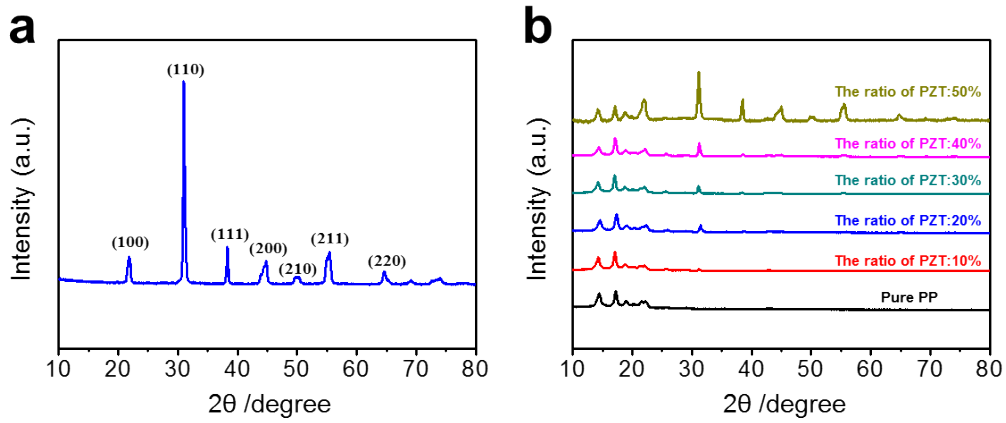


**Figure S5.** X-ray diffraction (XRD) of **(a)** PZT nanoparticles. **(b)** XRD spectrum of cellular PP/PZT composite film with different PZT doping ratios.

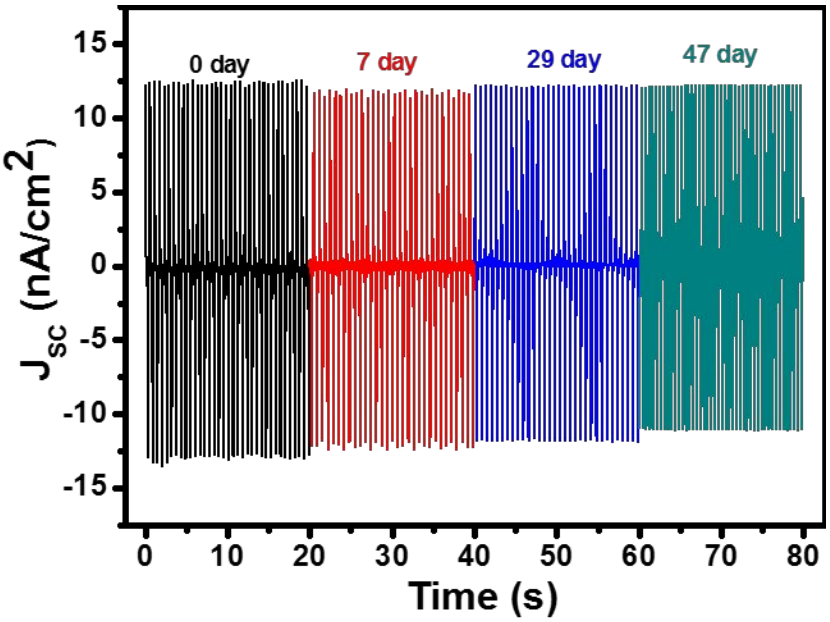


**Figure S6.** The 3D-CSA hold very stable electrical output in ambient enviroment.

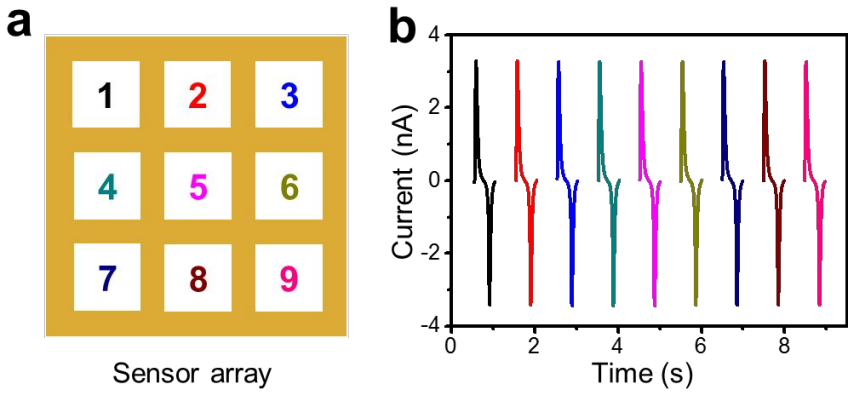


**Figure S7. The uniformity of the sensor array based on 3D-CSA**. **(a)** Digital labeling of array units. **(b)** The current output corresponding to each unit.

**Supporting Note 1: The physical model of 3D-CSA**

The 3D cellular PP electret with caged piezoelectric nanoparticles can be simplified as a hamburger structure with multi-layer. The structure comprises and *n+1* layers of PP with the thicknesses of $d_{2i}$ and $d_{1j}$ respectively, where$i = 1,2,...n$ and$j = 1,2,..n+1$. These layers are assumed to be laterally consensus, the top and bottom surface For the PNPFA in $i$ layer and PP in $j$ layer, if the direction of electric field $E$ from the bottom electrode to the top electrode was defined as the positive direction, the Gauss law can be written as:

$$-\varepsilon E_{1j} + E_{2i} = -\sigma_i/\varepsilon_0 \quad (1)$$

$$-E_{2i} + \varepsilon E_{1(j+1)} = \sigma_i/\varepsilon_0 \quad (2)$$

Where $\varepsilon$ and $\varepsilon_0$ and are the relative dielectric constant of PP and dielectric constant of PNPFA, separately. $E_{1j}$ and $E_{2i}$ represent the corresponding electric field of PP in $j$ layer and PEPFA in $i$ layer, respectively. Kirchhoff' law for short-circuit conditions can be written as:

$$\sum_{i=1}^{n} d_{2i}E_{2i} + \sum_{j=1}^{n+1} d_{1j}E_{1j} = 0 \quad (3)$$

Combining equations (a) and (b), simultaneous equation (c) yields $E_{11} = E_{12} = ...E_{1j} = E_{1(j+1)} = E_1$. And $E_1$ can be expressed as

$$E_1 = \frac{\sum_{i=1}^{n} d_{2i}\sigma_i}{\varepsilon_0(\varepsilon D_2 + D_1)} \quad (4)$$

Where$D_2 = \sum_{i=1}^{n} d_{2i}$, $D_1 = \sum_{i=1}^{n+1} d_{1j}$. For the convenience of analyzing, we hypothesized that each PNPFA layer has the same thickness, $d_{2i}$=$d_2$.then the charge density on the copper electrode $\sigma_0$ can be expressed as:

$$\sigma_0 = \varepsilon_0\varepsilon E_{1i} = \varepsilon_0\varepsilon E_1 = \frac{\varepsilon\sum_{i=1}^{n} d_{2i}\sigma_i}{\varepsilon D_2 + D_1} = \frac{\varepsilon_n^1\sum_{i=1}^{n}\sigma_i}{\varepsilon + {}^{D_1}/_{D_2}} \quad (5)$$

**Supporting Note 2**: **Structural optimization of the cellular PP framework**

The surface morphology of cellular PP framework formed by adding different proportions of dibutyl phthalate (DBP) in the weight ratio of 30% solution were compared in **Figure S8**. Owing to the differences of phase equilibrium and corresponding equilibrium thermodynamics in the varied weight ratio of DBP, the morphology appears in the form of non-microcellular morphology (Figure S8 **a**), cell clusters texture with a certain interlaced structure (Figure S8 **b**), honeycomb-shaped hole structure (Figure S8 **c**), the distance between the pores decreases and exhibits the enhanced compactness (Figure S8 **d**), rupture areas increase (Figure S8 **e**).

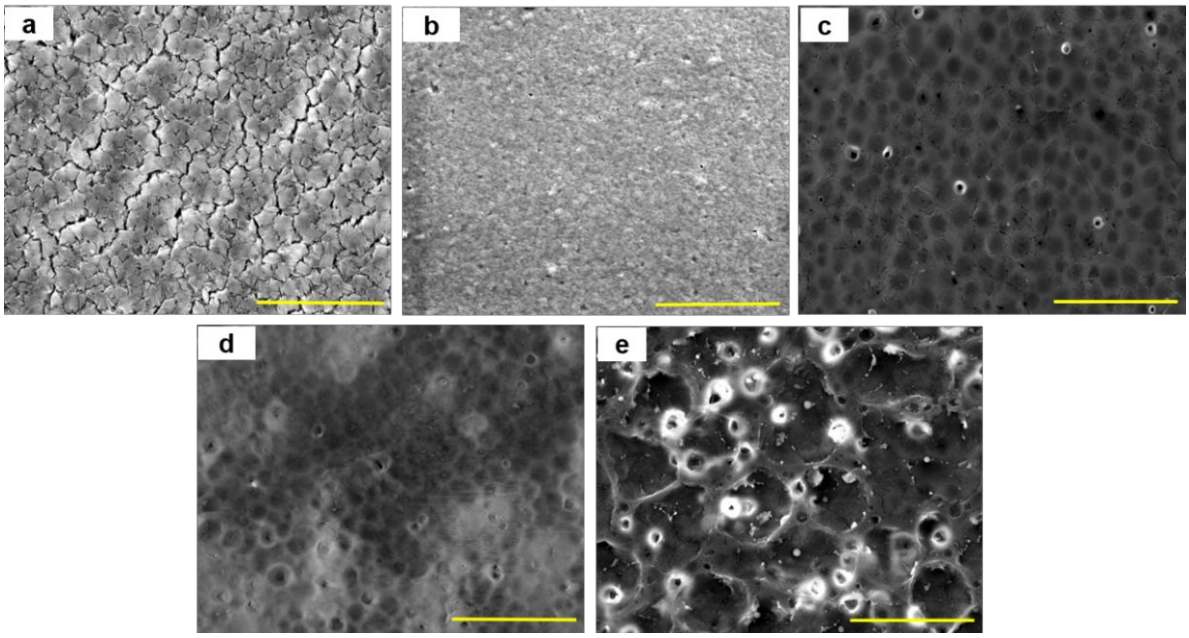


**Figure S8.** Field-emission scanning electron microscopy (FE-SEM) images of the cellular PP framework from 30 wt% solution with different weight ratios of DBP in mixed diluent, **(a)** 20%, **(b)** 40%, **(c)** 60%, **(d)** 80%, **(e)** 100%, respectively. The scale bars, 25 μm.

The piezoelectric properties of the cellular PP (**Figure S9**) indicates that when the weight ratio is 60%, the maximum value of voltage (Figure S9 **a**), current (Figure S9 **b**) and current density (Figure S9 **c**) are obtained. Such a tradeoff is attributed to a competitive effect between the enhancement of the piezoelectric properties arising from the increase of the capture centers for storing charges and the increase of leakage current caused by the increasing of inherent destruction in the cellular structure. The honeycomb and cellular structure in PP create interfaces that contain more complex local defects such as broken chains, double bonds and high concentrations of free radicals, thus resulting in a large number of capture centers for storing charges. Meanwhile, the discontinuous structure and gaps of the fibril structure will cause the transfer of de-hydrazine charges.

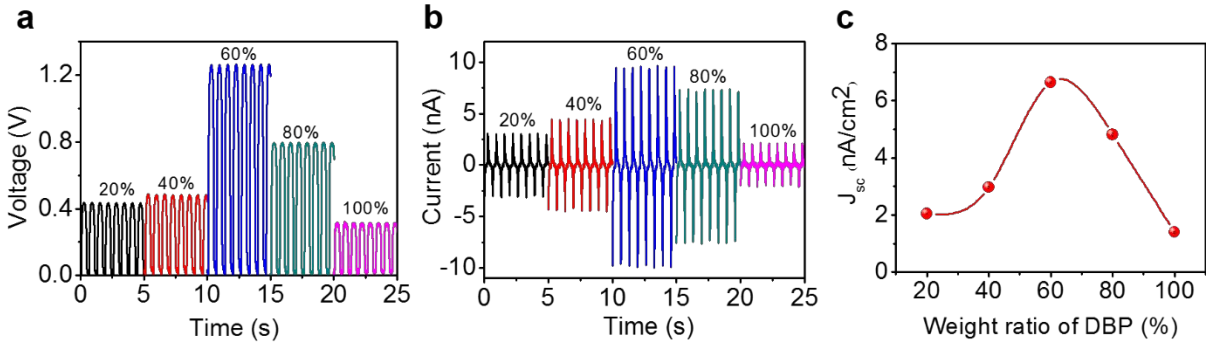


**Figure S9. (a)** The open-circuit voltage and **(b)** short-circuit current, **(c)** current density of the cellular PP electret sensor as a function of the mass fraction of dibutyl phthalate (DBP) in the mixed diluent.

When the weight ratio of DBP is less than 60%, the increase in the number of capture centers for storing charges is dominant with a stronger piezoelectric performance. On contrary, when the weight ratio exceeds 60%, the denting of cell structure and the increased areas of rupture brings a negative impact on piezoelectricity, leading to the reduction of the charges deposited in the void

layer after corona polarization with poorer piezoelectric performance. In a word, a 60% DBP weight ratio is the optimized design for 3D-CSA.

**Supporting Note 3: Performance optimization of cellular PP/PZT composite framework**

PZT filling into the pores of cellular forms a caged structure, with increasing ratio of PZT nanoparticle, the effective volume of the voids becomes smaller and impactful electrolysis separation volume of air in the hole is further reduced after corona polarization simultaneously, resulting in weak piezoelectric properties and reaches the minimum at the ratio of 20%. With further increase of the PZT content, the synergistic effects between alignment of dipole and ionization decomposition of the air in the pores make the electrical performance rise rapidly, and maximum value arrived when the ratio is 30% (**Figure S10**). Over this content, filling is close to saturation in the limited void space and the cellular structure begins to be destroyed, the contribution of polarization is mainly from the dipoles orientation of PZT, without the increment from hole, the synergistic effect disappeared and then the piezoelectricity reduced.

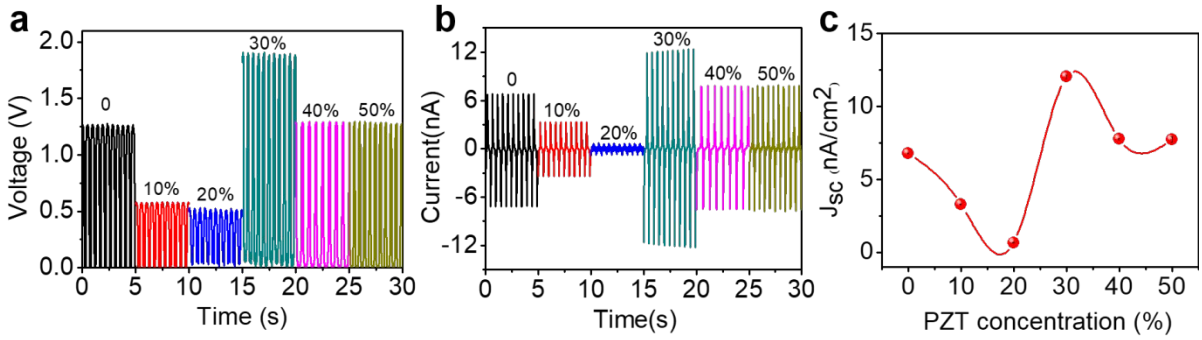


**Figure S10. (a)** The open-circuit voltage and **(b)** short-circuit current, **(c)** current density of 3D-CSA as a function of PZT doping ratio in a range from 0-50%.

**Table S1. Summary of the self-powered devices based on piezoelectric effect and their pressure sensitivity.**

| Mechanisms | Active materials | Pressure sensitivity | Ref. |
|---|---|---|---|
| Piezoelectricity | **Cellular PP/PZT** | **0.19 V $kPa^{-1}$ (0.475 V $N^{-1}$)** | **This work** |
| Piezoelectricity | P(VDF-TrFE)/BaTiO3 | 257.9 mV $N^{-1}$ | S1 |
| Piezoelectricity | ZnO Nanorods | 0.403 mV $kPa^{-1}$ | S2 |
| Piezoelectricity | ZnO Nanorods | 21.2 μV $kPa^{-1}$ | S3 |
| Piezoelectricity | P(VDF-TrFE) | 0.269 V $N^{-1}$ | S4 |
| Piezoelectricity | P(VDF-TrFE) nanowires | 0.458 V $N^{-1}$ | S5 |
| Piezoelectricity | P(VDF-TrFE) | 0.75 mV $kPa^{-1}$ | S6 |
| Piezoelectricity | Cellular PP/α-Si:H | 0.1 V $kPa^{-1}$ | S7 |
| Piezoelectricity | Polypropylene | 7.05 mV $N^{-1}$ | S8 |
| Piezoelectricity | PVDF | 7.64 mV $kPa^{-1}$ | S9 |
| Piezoelectricity | THV/COC | 30 mV $kPa^{-1}$ | S10 |

**References:**

(S1) Chen, X.; Li, X.; Shao, J.; An, N.; Tian, H.; Wang, C.; Han, T.; Wang, L.; Lu, B. High-Performance Piezoelectric Nanogenerators with Imprinted P(VDF-TrFE)/$BaTiO_3$ Nanocomposite Micropillars for Self-Powered Flexible Sensors. *Small* **2017**, 13, 1604245.

(S2) Deng, W.; Jin, L.; Zhang, B.; Chen, Y.; Mao, L.; Zhang, H.; Yang, W. A Flexible Field-Limited Ordered ZnO Nanorod-Based Self-Powered Tactile Sensor Array for Electronic Skin. *Nanoscale* **2016**, 8, 16302-16306.

(S3) Nabar, B. P.; Celik-Butler, Z.; Butler, D. P. Self-Powered Tactile Pressure Sensors Using Ordered Crystalline ZnO Nanorods on Flexible Substrates Toward Robotic Skin and Garments. *IEEE Sens. J.* **2015,** *15*, 63-70.

(S4) Chen, X.; Tian, H.; Li, X.; Shao, J.; Ding, Y.; An, N.; Zhou, Y. A High Performance P(VDF-TrFE) Nanogenerator with Self-Connected and Vertically Integrated Fibers by Patterned EHD Pulling. *Nanoscale* **2015**, 7, 11536-11544.

(S5) Chen, X.; Shao, J.; An, N.; Li, X.; Tian, H.; Xu, C.; Ding, Y. Self-Powered Flexible Pressure Sensors with Vertically Well-Aligned Piezoelectric Nanowire Arrays for Monitoring Vital Signs. *J. Mater. Chem. C.* **2015**, 3, 11806-11814.

(S6) Sharma, T.; Je, S.-S.; Gill, B.; Zhang, J. X. J. Patterning Piezoelectric Thin Film PVDF-TrFE Based Pressure Sensor for Catheter Application. *Sensor Actuat. A-Phys* **2012**, 177, 87-92.

(S7) Graz, I.; Kaltenbrunner, M.; Keplinger, C.; Schwödiauer, R.; Bauer, S.; Lacour, S. P.; Wagner, S. Flexible Ferroelectret Field-Effect Transistor for Large-Area Sensor Skins and Microphones. *Appl. Phys. Lett.* **2006**, 89, 073501.

(S8) Buchberger, G.; Schwödiauer, R.; Bauer, S. Flexible Large Area Ferroelectret Sensors for Location Sensitive Touchpads. *Appl. Phys. Lett.* **2008**, 92, 123511.

(S9) Deng, C.; Tang, W.; Liu, L.; Chen, B.; Li, M.; Wang, Z. L. Self -Powered Insole Plantar Pressure Mapping System. *Adv. Funct. Mater.* **2018**, 28, 1801606.

(S10) Li, W.; Duan, J.; Zhong, J.; Wu, N.; Lin, S.; Xu, Z.; Chen, S.; Pan, Y.; Huang, L.; Hu, B.; Zhou, J. Flexible THV/COC Piezoelectret Nanogenerator for Wide-Range Pressure Sensing. *ACS Appl. Mater. Inter.* **2018**, 10, 29675-29683.